





Light and Period Variations in Two K-type Contact Binaries: HI Leo and V523 Cas

Yuanguai Yang , Shuang Wang, Huiyu Yuan , and Haifeng Dai

School of Physics and Electronic Information, Huaibei Normal University, Huaibei 235000, China; yygc@163.com
Received 2022 September 4; revised 2022 September 22; accepted 2022 September 28; published 2022 November 29

Abstract

We presented a low-precision spectrum for HI Leo, Transiting Exoplanet Survey Satellite data for V523 Cas, and new photometry for both K-type contact binaries. Comparing their light curves on different observing dates, we found small intrinsic variabilities, such as variable amplitudes for HI Leo and the varying heights around the second maxima for V523 Cas. By the Wilson–Devinney Code, we deduced six photometric solutions. The dark spot of V523 Cas may appear on the surface of the more massive component on BJD 2458768, while it disappears on BJD 2458779. Our results indicate that the two binaries are W-type shallow-contact binaries ($f \leq 10\%$). From the eclipse timing residuals, we found that the orbital periods may continuously increase, accompanied by one to two light-time effects due to additional bodies. The modulated periods and semi-amplitudes are $P_3 = 25.8(\pm 1.0)$ yr and $A_3 = 0^d0066(6)$ for HI Leo, $P_3 = 114.8(\pm 2.0)$ yr and $A_3 = 0^d0448(12)$, $P_4 = 18.89(\pm 0.14)$ yr and $A_4 = 0^d0025(2)$ for V523 Cas, respectively. The orbital period secularly increases at a rate of $dP/dt = 2.86(\pm 0.11) \times 10^{-7}$ day yr $^{-1}$ for HI Leo and $dP/dt = 3.45(\pm 0.07) \times 10^{-8}$ day yr $^{-1}$ for V523 Cas, which may be attributed to mass transfer from the secondary to the primary. With mass transferring, the shallow-contact binaries, HI Leo and V523 Cas, will evolve into the broken-contact configurations.

Key words: (stars:) binaries (including multiple): close – (stars:) binaries: eclipsing – stars: activity

Online material: machine-readable table

1. Introduction

W UMa binaries contain two low-mass components filling their Roche lobes with common envelopes. They are the most frequently observed objects due to their short periods and comprehensive distribution, which provide fundamental stellar parameters from light curves (LCs) and radial velocity (RV) curves (Andersen 1991). Several investigators (Eggleton 2010; Stępień 2011; Langer 2012) reviewed theoretical and observational studies for contact binaries. They may be formed from moderate close binaries (Qian et al. 2017), may have gone through the mass ratio reversal with mass loss, angular momentum transfer and loss (Stępień & Gazeas 2008). They finally merge into a single star like the known star V1309 Sco (Tylenda et al. 2011; Zhu et al. 2016). Contact binaries may suffer cyclic thermal relaxation oscillation (TRO) between contact and semi-detached states, which was summarized by Webbink (2003). Recently, several statistical studies of contact binaries have been performed by Qian et al. (2020), Kouzuma (2019), Liu et al. (2018). Based on the LAMOST spectral survey, Zhang et al. (2018) studied stellar spectroscopic properties and chromospheric activity, 34 of which are eclipsing binaries. Kouzuma (2019) suggested that the magnetic activity caused by stellar dynamos should form the cool spots in W-type contact binaries. Latković et al. (2021) carried out a

study of 700 W UMa binaries and obtained a series of statistical relations between parameters of binaries. A dozen of short-period contact binaries with magnetic activities have been observed by Long et al. (2019), Zhang et al. (2020a) and Yang et al. (2022). They studied the dark spot immigrating on the stellar surface inferred from asymmetric light curves. This paper focused on two active contact binaries, HI Leo and V523 Cas, to explore the intrinsic light and period variations.

V523 Cas (TIC 240706234, $V = 10.87$ mag) is a short-period (~ 0.237 day), cool eclipsing variable star, which was found by Weber (1957). Its spectral type is K4V (Bradstreet 1981; Rucinski et al. 2003). Zhang & Zhang (2004) and Mohammadi et al. (2016) successively reviewed the history of this W-type binary. Milone et al. (1985) first performed a radial-velocity study and gave a mass ratio of $q_{\text{sp}} = 0.42(\pm 0.02)$ and velocity semi-amplitudes of $K_1 = 96(\pm 5)$ and $K_2 = 231(\pm 4)$ km s $^{-1}$. More than 20 yr later, Rucinski et al. (2003) updated a mass ratio of $q_{\text{sp}} = 0.516(\pm 0.007)$ and $K_1 = 121.64(\pm 1.14)$ km s $^{-1}$ and $K_2 = 235.95(\pm 1.41)$ km s $^{-1}$, respectively. Photometric studies for V523 Cas have been done at least 15 times in the literature. From the (un)spotted solutions (Zhang & Zhang 2004; Zola et al. 2010), the fill-out factor varies from 30.4% (Mohammadi et al. 2016) to 4.82% (Zboril & Djurasevic 2006). Based on the eclipse residuals, the orbital period

variations have been analyzed by numerous authors, who gave some different results, such as period increase (Zhang & Zhang 2004), together with one cyclic oscillation (Rovithis-Livaniou et al. 2003; Samec et al. 2004) or two ones (Mohammadi et al. 2016; Maithong 2021).

Another object HI Leo (=1RXS J111218.0+011907, $V = 11.06$ mag) is a suspected variable star in the Sloan Digital Sky Survey (SDSS) calibration fields (Henden & Stone 1998). Greaves & Wils (2003) classified it as an EW-type eclipsing binary with a period of 0.31158 day. Szczygiel et al. (2008) obtained a ratio of soft X-ray to the bolometric luminosity of $L_X/L_{\text{bol}} = 3.98 \times 10^{-4}$, which implies that HI Leo may display a coronal active. Agueros et al. (2009) then listed it as an X-ray-emitting star. Although many eclipse times are monitored, no information on photometry and spectroscopy for HI Leo has been published up to now.

In this paper, the spectrum of HI Leo, Transiting Exoplanet Survey Satellite (TESS) survey data of V523 Cas,¹ and new photometry of two binaries, are presented in Section 2. Based on all available eclipse timings, we studied the orbital period variations in Section 3. In Section 4, we first compared the light curves with different observing dates and then deduced several sets of photometric elements by the Wilson–Devinney (W-D) program.² Finally, we (re)determined the absolute parameters for two binaries and discussed the evolutionary scenarios and additional companions.

2. Observations

2.1. Low-precision Spectrum for HI Leo

On 2017 January 22, we observed this binary using the *BFOSC* instrument of the 2.16 m telescope at the Xinglong station (XLs) of the National Astronomical Observatories, Chinese Academy of Sciences (NAOC). During the observation, we chose the slit width of $1''.8$ and the *Grism-3* with a reciprocal linear dispersion of $\sim 139 \text{ \AA mm}^{-1}$ (Fan et al. 2016). The exposure time for this star is 10 minutes. A low-precision spectrum for HI Leo was reduced by the *IRAF* packages,³ including bias subtraction, flat-fielding and removing the cosmic-ray. Then we obtained a one-dimension spectrum. Using the *wink* software,⁴ we obtained the final normalized spectrum, which is shown in Figure 1. With the comparison with the spectra of standard stars (Pickles 1998), HI Leo should be a K2V-type binary.

¹ <https://mast.stsci.edu/portal/Mashup/Clients/Mast/Portal.html>

² <ftp.astro.ufl.edu/pub/wilson/lcdc2015/>

³ IRAF is supported by the National Optical Astronomy Observatories (NOAO) in Tucson, Arizona, which may available from <http://iraf.noao.edu/iraf/web/iraf-homepage.html>.

⁴ <http://www.appstate.edu/~grayro/MK/winkm.htm>

2.2. Ground-base Photometry

New photometry for HI Leo and V523 Cas was carried out on 11 nights from 2006 December to 2022 February using the 60 and 85 cm (Zhou et al. 2009) telescopes at the XLs of NAOC and the 1.0 m telescope at Yunnan Astronomical Observatory (YNAO). The standard Johnson–Cousins $UBVR_cI_c$ photometric systems were equipped with three telescopes. Photometric reduction for all observed images was performed by the *CCDRED* and *APPHOT* packages of IRAF.

The observing information for HI Leo and V523 Cas is given in Table 1, including comparison star and check star, observing dates, exposure times, the points of light curves and initial epoch times. We obtained the differential magnitudes, in terms of *variable minus comparison* and *check minus comparison*, and their corresponding heliocentric Julian dates. All individual data are available on request. Complete light curves for two binaries are displayed in Figure 2, whose phases are computed by the epoch times and orbital periods (Kreiner 2004). For HI Leo, we obtained three sets of light curves, i.e., LC_{2020} in the *BV* bands, LC_{2022} in the *BVRc* bands, and LC_{2015} in the *Rc* band on 2015 January 8 and 11.⁵ Meanwhile, the light curves in 2006 and 2007 only include 83 and 67 points in the *V* and *Rc* bands, so the time resolutions of data are very low. By the K-W method (Kwee & van Woerden 1956), we obtained some light minimum times from new photometric data, which are given in Table 2.

2.3. TESS Survey Data for V523 Cas

We freely downloaded the TESS observations by the MAST (Ricker et al. 2015). The observing dates began on 2019 October 8, and ended on 2019 November 11. We adopted the *SAP_FLUXes* for this binary and obtained 16,907 data with 2 minutes cadence. The continuous observations occur a 1.5 days gap between BJD 2458776.3 and BJD 2458777.7. To explore the intrinsic light variability, we computed the differences between two light maxima or minima (i.e., $\Delta M_{\text{max}} = \text{Max.I} - \text{Max.II}$ and $\Delta M_{\text{min}} = \text{Min.I} - \text{Min.II}$) in one period. Figure 3(a) exhibits ΔM_{max} and ΔM_{min} with time. The average value of ΔM_{min} is $0.091(\pm 0.003)$ mag indicates that the temperatures of the two components slightly differ. From its upper panel, ΔM_{max} gradually increases and then tends to be invariant, which implies that the O’Connell effect (O’Connell 1951) varies from negative to near zero. The dark spot may immigrate on the stellar surface or disappear. As shown in Figure 3(b), we intercepted two sections of light curves spanning one day, i.e., TIC_{1768} with $\Delta M_{\text{max}} = -0.014$ mag and TIC_{1779} with $\Delta M_{\text{max}} \simeq 0$. From TESS data, moreover, we determined 200 eclipse timings, listed in Table 3.

⁵ Other data in *Rc*-band data on 2005 January 9 and 10 were only used to determine the eclipse timing due to large scatter.

Table 1
Observing Log and Main Feature Parameters of Light Curves

Variable Star	HI Leo			V523 Cas (LC_{VRc})	
	LC_{2020}	LC_{2022}	LC_{2015}	LC_{2006V}	LC_{2007Rc}
Comparison star		TYC 263-121-1		TYC 3257-1326-1	
Check star		TYC 263-142-1		TYC 3257-1068-1	
Telescopes	60 cm	60 cm	60 cm	1.0 m	85 cm
Observing dates	2020 Feb 21 and 23	2022 Jan 28 (BV) and Feb 27 (BV)	2015 Jan 8, 9, 10 and 11	2006 Dec 12 and 14	2007 Nov 27
		2022 Feb 25 (Rc) and Mar 26 (V)			
Exposure times	60 s (B), 50 s (V)	40 s (B), 30 s (V), 50 s (Rc)	20 s (Rc)	90 s (V)	30 s (Rc)
Number of data	320 (B), 319 (V)	129(B), 281(V), 172(Rc)	1183 (Rc)	83(V)	67(Rc)
Epoch time (t_0)	HJD 2458903.3135	HJD 2459665.1641	HJD 2457034.3823	HJD 2454436.0534	
Period (day)		0.3115929		0.23369445	
Min.I – Max.II	+ 0 ^m .818 (B), + 0 ^m .774 (V)	+ 0 ^m .831 (V), + 0 ^m .768 (Rc)	+ 0 ^m .727 (Rc)	+ 0 ^m .799 (V)	+ 0 ^m .756 (Rc)
Max.I – Max.II	– 0 ^m .004 (B), – 0 ^m .005 (V)	+ 0 ^m .033 (B), + 0 ^m .015 (V), + 0 ^m .012 (Rc)	– 0 ^m .004 (Rc)	+ 0 ^m .024 (V)	– 0 ^m .009 (Rc)
Min.I – Min.II	+ 0 ^m .213 (B), + 0 ^m .204 (V)	+ 0 ^m .257 (V)	+ 0 ^m .171 (Rc)	+ 0 ^m .108 (V)	+ 0 ^m .176 (Rc)

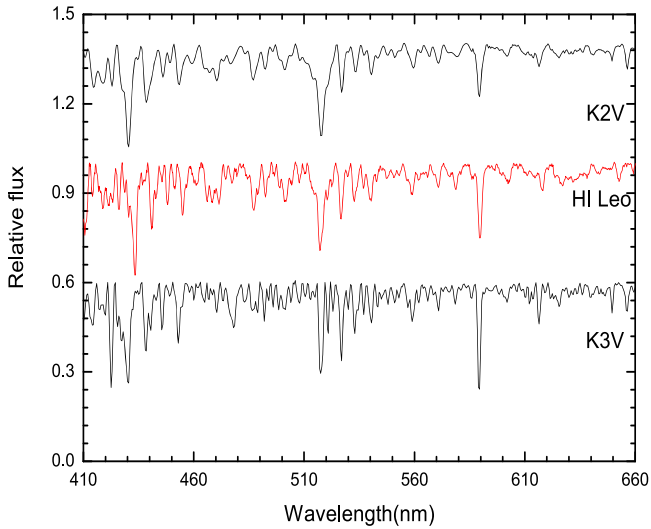


Figure 1. The low-precision spectrum of HI Leo, which was observed by the 2.16 m telescope at XLs of NAOC.

3. Orbital Period Analysis

For HI Leo and V523 Cas, we accumulated all available eclipse timings from the literature and new determined data. To study the period variations, we computed the eclipse timing residuals, whose naming was suggested by Wilson (2020). We applied the nonlinear least-squares fitting method with weights, which are inversely proportional to the squared errors. If the standard deviation losses in literature, we adopted an average value of all other data in the same observed method.

3.1. HI Leo

We collected all times of minimum light, including 15 visual measurements, four photometric and 46 CCD data and one ASAS epoch, which are listed in Table 4. With the linear ephemeris (Kreiner 2004),

$$\text{Min.I} = \text{HJD } 2452500.125 + 0.3115899 \times E, \quad (1)$$

we can compute the initial residuals, $(O - C)_i$, displayed in Figure 4(a). This figure shows that the $(O - C)_i$ curve exhibits a secular period increase with some oscillations. Therefore, the initial residuals are described by the following equation,

$$\text{Min.I} = T_0 + P \times E + Q \times E^2 + \tau \quad (2)$$

and

$$\tau = A \times \left[\frac{1 - e^2}{1 + e \cos \nu} + e \sin \nu \right], \quad (3)$$

where T_0 , P and Q are initial epoch time, orbital period and its changing rate. In Equation (3), $A = a_{12} \sin i/c$ is a semi-amplitude of light-time effect (LTE). Other parameters, a_{12} , e , i , ω and ν , are the orbital parameters for the additional pair (Irwin 1952). Adopting the nonlinear least-squared method (Yang 2009), we simultaneously derived seven parameters and their uncertainties, which are listed in Table 5. The final residuals $(O - C)_f$ are given in Table 4 and in Figure 4(b). Although the visual data scatter largely, the eclipse timing residuals are fitted well.

3.2. V523 Cas

Based on the different databases of eclipse times, some authors have analyzed its orbital period variations and given

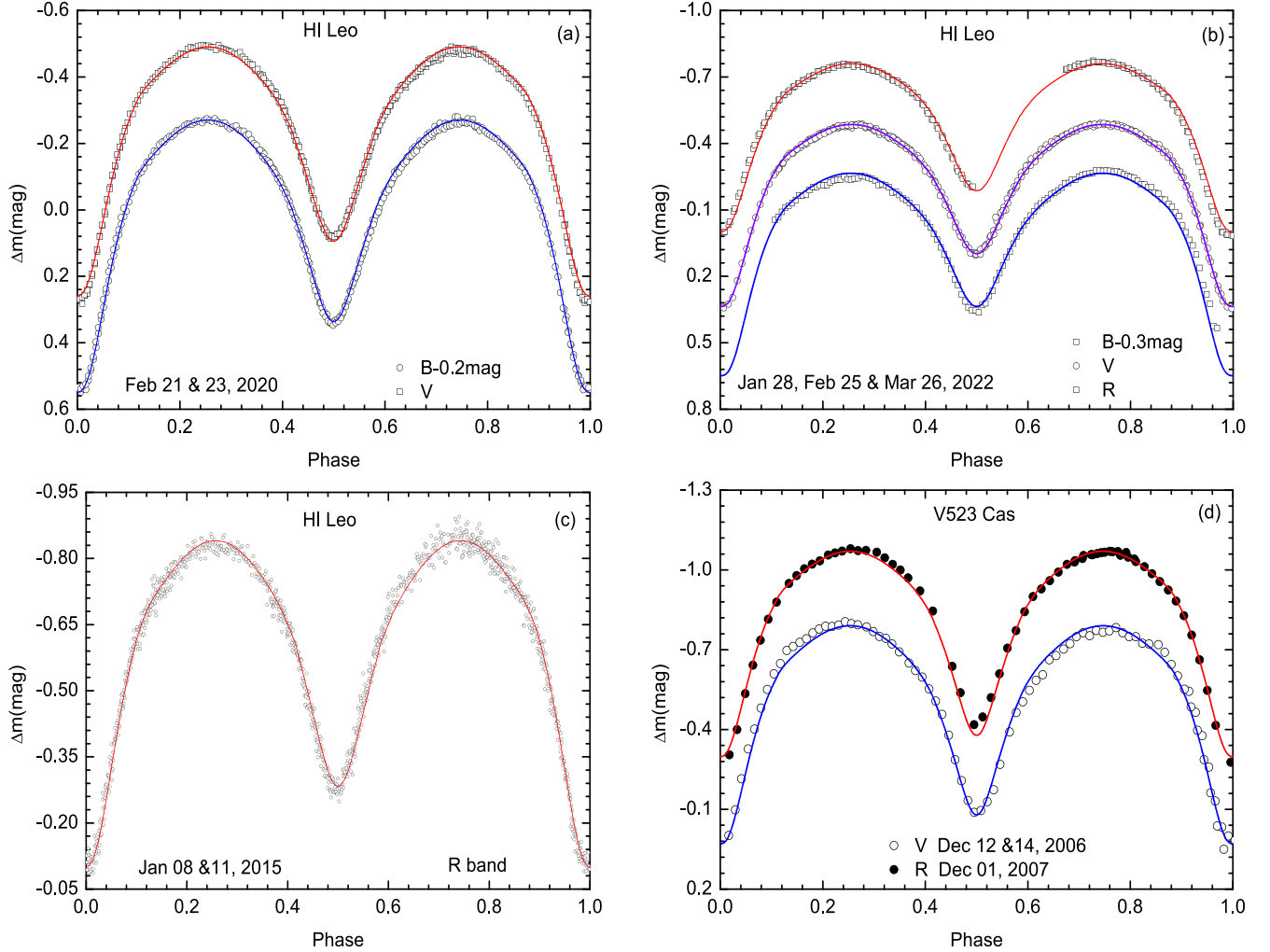


Figure 2. New light curves for two contact binaries, HI Leo (a)–(c) and V523 Cas (d). Theoretical light curves are plotted as continuous lines by the photometric solutions in Table 4.

different results (Rovithis-Livaniou et al. 2003; Mohammadi et al. 2016; Maithong 2021). Most of the eclipse times are listed in the literature, such as Kreiner et al. (2001), Zhang & Zhang (2004), and the $O - C$ gateway.⁶ We compiled a total of 769 ground-based eclipse timings, listed in Table 6, and 200 TESS eclipsing times in Table 3. Before being used, the TESS data were converted from BJD to HJD by *Time Unlites* (Eastman et al. 2010).⁷ All eclipse timings cover 120 yr, which may be one of the close binaries with long observed history. Using Zhang & Zhang (2004)’s linear ephemeris,

$$\text{Min.I} = \text{HJD } 2446708.7768 + 0.23369162 \times E, \quad (4)$$

we obtained the initial eclipse residuals $(O - C)_i$, which are listed in Table 6. The corresponding eclipse timing residuals

are displayed in Figure 5(a). Similarly to HI Leo, the $(O - C)_i$ for V523 Cas may be described by Equation (2). The fitted parameters are listed in Table 5. The modulated period of $P_3 = 114.8(\pm 2.0)$ yr is slightly longer than $P_3 = 101 \pm 5$ yr from Samec et al. (2004).

After the initial residuals were removed by Equation (2), the remained residuals, $(O - C)_1$, are displayed in the upper panel of Figure 5(b), not including low-precision photographic and visual data. There exists another cyclic variation, as suggested by Maithong (2021), Mohammadi et al. (2016). So we used another light-time effect with zero-point to fit $(O - C)_1$. The fitted parameters are also tabulated in Table 5. The final residuals $(O - C)_f$ are displayed in the lower panel of Figure 5(b). Except for the residuals before the 1990 scatter, most eclipse timing residuals are fitted well. Another modulated period of $P_4 = 18.89(\pm 0.14)$ yr is shorter than $P_4 = 29.35(\pm 0.81)$ yr deduced by Mohammadi et al. (2016). This situation with two

⁶ <http://var2.astro.cz/ocgate/>

⁷ <https://astrutils.astronomy.osu.edu/time/>

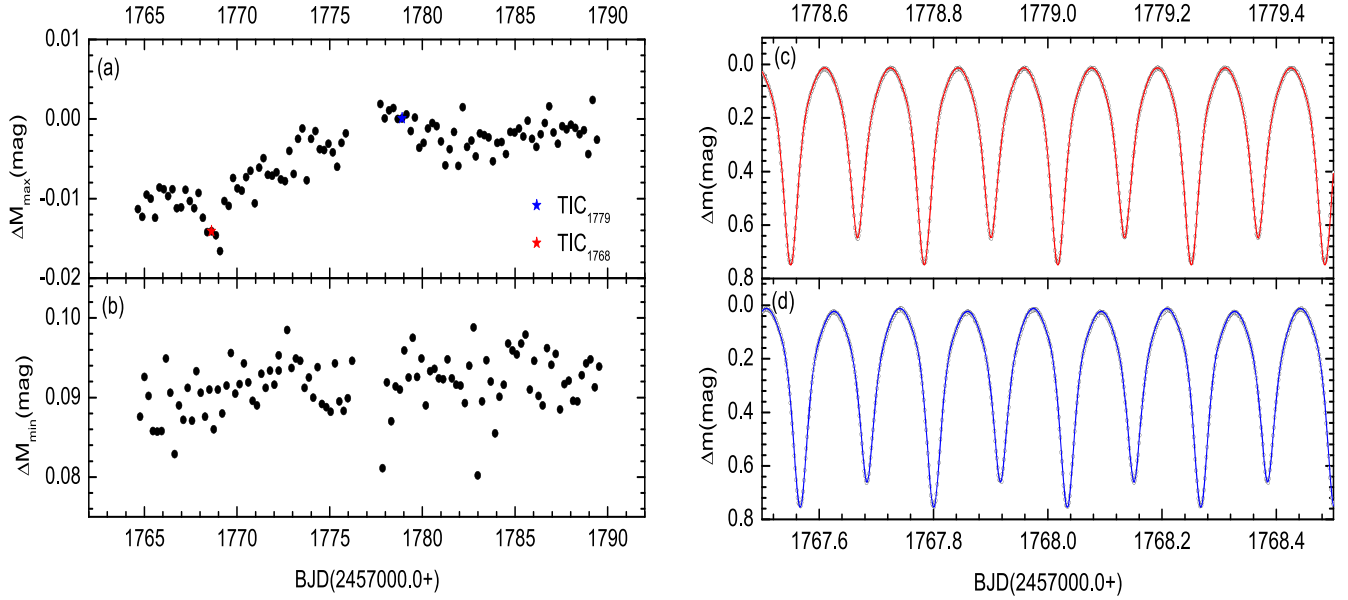


Figure 3. The differences between two light maxima/minima for V523 Cas, ΔM_{\max} (a) and ΔM_{\min} (b), from the TESS data. Comparing observed and theoretical light curves for TIC₁₇₇₉ (c) and TIC₁₇₆₈ (d).

Table 2
New Obtained Light Minimum Times

Star	HJD	Error	Type	Band	Telescopes
	2457031.26661	±0.00012	I	<i>B</i>	60 cm
	2457031.42170	±0.00014	II	<i>B</i>	60 cm
	2457032.35630	±0.00026	II	<i>B</i>	60 cm
	2457033.29202	±0.00031	II	<i>V</i>	60 cm
	2457034.22592	±0.00017	II	<i>V</i>	60 cm
	2457034.38225	±0.00013	I	<i>V</i>	60 cm
	2458901.13297	±0.00008	I	<i>B</i>	60 cm
	2458901.13262	±0.00008	I	<i>V</i>	60 cm
	2458901.28836	±0.00012	II	<i>B</i>	60 cm
	2458901.28845	±0.00009	II	<i>V</i>	60 cm
HI Leo	2458903.15796	±0.00007	II	<i>B</i>	60 cm
	2458903.15788	±0.00007	II	<i>V</i>	60 cm
	2458903.31341	±0.00008	I	<i>B</i>	60 cm
	2458903.31358	±0.00007	I	<i>V</i>	60 cm
	2459608.29841	±0.00015	II	<i>B</i>	60 cm
	2459608.29849	±0.00013	II	<i>V</i>	60 cm
	2459636.18556	±0.00009	I	<i>V</i>	60 cm
	2459638.21122	±0.00044	II	<i>B</i>	60 cm
	2459638.21047	±0.00042	II	<i>V</i>	60 cm
	2459665.16412	±0.00030	I	<i>V</i>	60 cm
<hr/>					
	2454082.00982	±0.00014	I	<i>V</i>	1.0 m
	2454082.12758	±0.00017	II	<i>V</i>	1.0 m
	2454431.63187	±0.00023	I	<i>B</i>	85 cm
V523 Cas	2454431.63210	±0.00014	I	<i>V</i>	85 cm
	2454431.63209	±0.00020	I	<i>Rc</i>	85 cm
	2454436.05530	±0.00036	I	<i>Rc</i>	85 cm
	2454436.17151	±0.00025	I	<i>Rc</i>	85 cm

periods may occur in other binaries, such as OO Aql (Li et al. 2016) and RW Com (Özavic et al. 2020). Certainly, the complicated variations for this binary are still being checked in future observations.

4. Photometric Analyses

4.1. Intrinsic Light Variability

From our new light curves and TESS ones, we qualified their main feature parameters, which are listed in Table 1, including the variable light amplitude ($\Delta M_{\text{var}} = \text{Min.I} - \text{Max.I}$), and the difference between light maxima or minima, ΔM_{\max} or ΔM_{\min} .

As displayed in Figure 6(a), we compared the *V*-band light curves LC₂₀₂₀ and LC₂₀₂₂ for HI Leo. ΔM_{var} becomes larger and the secondary eclipse shallower from 2020 to 2022. Light curves of LC₂₀₂₀ are symmetric, while LC₂₀₂₂ could not cover an entire period except in the *V* band. For V523 Cas, ΔM_{\max} are 0^m.024 (*V*) in LC₂₀₂₂ and −0^m.009 (*Rc*) in LC₂₀₀₇, which identified the unequal heights of two light maxima (Zhang & Zhang 2004). From Figure 6(b), a small intrinsic light variability occurs in phase 0.75 from two sections of TESS light curves, i.e., TIC₁₇₆₈ and TIC₁₇₇₉. This kind of short timescale variability also happens in other contact binaries, such as EE Cet (Yang & Wang 2023), and QR Com (Wang & Yuanguai 2023), which implies that a cool spot immigrates or disappears on the surface of the active star.

Table 3
Light Minimum Times of V523 Cas from TESS

Primary Time				Secondary Times			
BJD (2457000+)	Error	BJD (2457000+)	Error	BJD (2457000+)	Error	BJD (2457000+)	Error
1764.76215	±0.00004	1778.08274	±0.00009	1764.87915	±0.00008	1778.19967	±0.00009
1764.99606	±0.00009	1778.31645	±0.00009	1765.11286	±0.00013	1778.43337	±0.00005
1765.22977	±0.00008	1778.55007	±0.00006	1765.34647	±0.00007	1778.66685	±0.00007
1765.46343	±0.00013	1778.78390	±0.00006	1765.58029	±0.00010	1778.90076	±0.00004
1765.69715	±0.00012	1779.01742	±0.00013	1765.81393	±0.00008	1779.13441	±0.00005
1765.93084	±0.00009	1779.25117	±0.00012	1766.04754	±0.00008	1779.36812	±0.00005
1766.16434	±0.00006	1779.48488	±0.00007	1766.28138	±0.00011	1779.60185	±0.00007
1766.39808	±0.00005	1779.71860	±0.00009	1766.51487	±0.00009	1779.83552	±0.00008
1766.63184	±0.00005	1779.95230	±0.00009	1766.74863	±0.00009	1780.06928	±0.00006
1766.86556	±0.00010	1780.18590	±0.00007	1766.98254	±0.00011	1780.30290	±0.00013
1767.09927	±0.00007	1780.41956	±0.00010	1767.21615	±0.00009	1780.53657	±0.00004
1767.33285	±0.00005	1780.65332	±0.00007	1767.44981	±0.00009	1780.77022	±0.00007
1767.56658	±0.00011	1780.88697	±0.00006	1767.68344	±0.00009	1781.00405	±0.00011
1767.80033	±0.00007	1781.12070	±0.00005	1767.91726	±0.00023	1781.23765	±0.00007
1768.03405	±0.00010	1781.35440	±0.00007	1768.15093	±0.00010	1781.47134	±0.00003
1768.26764	±0.00005	1781.58806	±0.00005	1768.38466	±0.00018	1781.70510	±0.00005
1768.50138	±0.00006	1781.82182	±0.00008	1768.61826	±0.00008	1781.93872	±0.00006
1768.73511	±0.00008	1782.05555	±0.00009	1768.85191	±0.00012	1782.17246	±0.00003
1768.96869	±0.00004	1782.28924	±0.00007	1769.08571	±0.00010	1782.40609	±0.00006
1769.20248	±0.00005	1782.52287	±0.00011	1769.31935	±0.00017	1782.63981	±0.00004
1769.43615	±0.00005	1782.75655	±0.00010	1769.55298	±0.00008	1782.87354	±0.00006
1769.66991	±0.00008	1782.99037	±0.00007	1769.78678	±0.00011	1783.10722	±0.00012
1769.90344	±0.00005	1783.22388	±0.00008	1770.02047	±0.00011	1783.34087	±0.00004
1770.13715	±0.00005	1783.45763	±0.00006	1770.25390	±0.00009	1783.57462	±0.00006
1770.37093	±0.00005	1783.69133	±0.00010	1770.48788	±0.00015	1783.80827	±0.00005
1770.60457	±0.00004	1783.92496	±0.00015	1770.72162	±0.00011	1784.04190	±0.00012
1770.83829	±0.00006	1784.15879	±0.00008	1770.95521	±0.00010	1784.27564	±0.00005
1771.07203	±0.00006	1784.39243	±0.00005	1771.18871	±0.00010	1784.50939	±0.00005
1771.30559	±0.00007	1784.62614	±0.00005	1771.42267	±0.00012	1784.74301	±0.00005
1771.53937	±0.00004	1784.85977	±0.00009	1771.65637	±0.00012	1784.97679	±0.00004
1771.77308	±0.00007	1785.09352	±0.00007	1771.89006	±0.00011	1785.21049	±0.00006
1772.00679	±0.00011	1785.32723	±0.00006	1772.12352	±0.00009	1785.44409	±0.00005
1772.24046	±0.00005	1785.56085	±0.00009	1772.35734	±0.00008	1785.67786	±0.00008
1772.70787	±0.00005	1785.79458	±0.00007	1772.59115	±0.00011	1785.91152	±0.00007
1772.94145	±0.00005	1786.02819	±0.00015	1772.82477	±0.00010	1786.14523	±0.00009
1773.17504	±0.00006	1786.26192	±0.00007	1773.05844	±0.00008	1786.37891	±0.00005
1773.40889	±0.00004	1786.49568	±0.00010	1773.29212	±0.00009	1786.61265	±0.00003
1773.64263	±0.00007	1786.72932	±0.00007	1773.52593	±0.00009	1786.84629	±0.00004
1773.87629	±0.00007	1786.96304	±0.00005	1773.75962	±0.00009	1787.07995	±0.00004
1774.11003	±0.00009	1787.19670	±0.00007	1773.99338	±0.00014	1787.31371	±0.00004
1774.34364	±0.00005	1787.43032	±0.00012	1774.22695	±0.00007	1787.54742	±0.00004
1774.57729	±0.00004	1787.66412	±0.00009	1774.46056	±0.00008	1787.78106	±0.00007
1774.81109	±0.00007	1787.89771	±0.00018	1774.69438	±0.00010	1788.01474	±0.00002
1775.04473	±0.00005	1788.13148	±0.00006	1774.92803	±0.00009	1788.24843	±0.00008
1775.27856	±0.00007	1788.36522	±0.00009	1775.16185	±0.00013	1788.48215	±0.00014
1775.51218	±0.00013	1788.59889	±0.00011	1775.39549	±0.00010	1788.71583	±0.00009
1775.74585	±0.00006	1788.83266	±0.00009	1775.62914	±0.00009	1788.94945	±0.00006
1775.97949	±0.00007	1789.06624	±0.00009	1775.86285	±0.00009	1789.18319	±0.00009
1776.21330	±0.00009	1789.30006	±0.00005	1776.09647	±0.00009	1789.41688	±0.00006
1777.84907	±0.00008	1789.53370	±0.00009	1777.96588	±0.00006	1789.65055	±0.00004

Table 4
All Available Light Minimum Times for HI Leo

JD(Hel.)	Error	Epoch	Method	Type	$(O - C)_i$ (days)	$(O - C)_f$ (days)	References
2450549.4292	± 0.0002	-6260.5	CCD	II	+0.0128	+0.0002	(1)
2450551.4537	± 0.0011	-6254.0	CCD	I	+0.0119	-0.0007	(1)
2451871.033	...	-2019.0	...	I	+0.0080	-0.0006	(2)
2452740.680	...	+772.0	pe	I	+0.0076	+0.0012	(3)
2452997.739	± 0.004	1597.0	vi	I	+0.0049	-0.0007	(4)
2453048.525	± 0.007	1760.0	vi	I	+0.0018	-0.0037	(4)
2453052.583	± 0.002	1773.0	vi	I	+0.0091	+0.0036	(4)
2453063.490	± 0.002	1808.0	vi	I	+0.0105	+0.0050	(4)
2453079.373	± 0.002	1859.0	vi	I	+0.0024	-0.0030	(4)
2453080.629	± 0.004	1863.0	vi	I	+0.0120	+0.0066	(4)
2453092.462	± 0.003	1901.0	vi	I	+0.0046	-0.0008	(4)
2453093.393	± 0.001	1904.0	vi	I	+0.0008	-0.0045	(4)
2453110.534	± 0.002	1959.0	vi	I	+0.0044	-0.0009	(4)
2453116.454	± 0.002	1978.0	vi	I	+0.0042	-0.0011	(4)
2453150.415	± 0.003	2087.0	vi	I	+0.0019	-0.0033	(4)
2453346.712	± 0.003	2717.0	vi	I	-0.0028	-0.0073	(4)
2453347.652	± 0.002	2720.0	vi	I	+0.0025	-0.0021	(4)
2453464.496	± 0.002	3095.0	vi	I	+0.0003	-0.0040	(4)
2453465.433	± 0.001	3098.0	vi	I	+0.0025	-0.0017	(4)
2454507.5420	± 0.0001	6442.5	CCD	II	-0.0009	-0.0020	(5)
2454555.3732	± 0.0001	6596.0	pe	I	+0.0012	+0.0003	(6)
2454862.9147	± 0.0006	7583.0	CCD	I	+0.0035	+0.0032	(7)
2454923.3602	± 0.0001	7777.0	pe	I	+0.0006	+0.0004	(8)
2454935.3569	± 0.0002	7815.5	CCD	II	+0.0010	+0.0009	(9)
2455232.1452	...	8768.0	CCD	I	+0.0000	+0.0004	(10)
2455232.3005	...	8768.5	CCD	II	-0.0005	-0.0001	(10)
2455268.1328	...	8883.5	CCD	II	-0.0011	-0.0006	(10)
2455268.2889	...	8884.0	CCD	I	-0.0008	-0.0003	(10)
2455268.9122	± 0.0001	8886.0	CCD	I	-0.0006	-0.0002	(11)
2455591.8746	± 0.0003	9922.5	CCD	II	-0.0012	-0.0004	(12)
2455597.4846	± 0.0017	9940.5	CCD	II	+0.0002	+0.0010	(13)
2455672.7336	± 0.0003	10182.0	CCD	I	+0.0002	+0.0011	(12)
2455941.9466	± 0.0001	11046.0	CCD	I	-0.0004	+0.0004	(14)
2455956.9040	± 0.0002	11094.0	CCD	I	+0.0006	+0.0015	(15)
2456029.9714	...	11328.5	CCD	II	+0.0002	+0.0010	(16)
2456035.7362	± 0.0002	11347.0	CCD	I	+0.0006	+0.0014	(15)
2456364.1506	...	12401.0	CCD	I	-0.0008	-0.0003	(17)
2456364.3051	...	12401.5	CCD	II	-0.0020	-0.0016	(17)
2457031.2666	± 0.0001	14542.0	CCD	I	+0.0013	+0.0000	(18)
2457031.4217	± 0.0001	14542.5	CCD	II	+0.0006	-0.0007	(18)
2457032.3563	± 0.0003	14545.5	CCD	II	+0.0004	-0.0009	(18)
2457033.2920	± 0.0003	14548.5	CCD	II	+0.0014	+0.0001	(18)
2457034.2259	± 0.0002	14551.5	CCD	II	+0.0005	-0.0008	(18)
2457034.3822	± 0.0001	14552.0	CCD	I	+0.0010	-0.0003	(18)
2457069.1241	...	14663.5	CCD	II	+0.0006	-0.0008	(19)
2457069.2807	...	14664.0	CCD	I	+0.0014	+0.0000	(19)
2457079.4064	± 0.0002	14696.5	pe	II	+0.0004	-0.0011	(20)
2457110.7238	± 0.0001	14797.0	CCD	I	+0.0031	+0.0014	(21)
2457398.3213	...	15720.0	CCD	I	+0.0031	+0.0001	(22)
2457492.7329	± 0.0001	16023.0	CCD	I	+0.0029	-0.0006	(23)
2457806.0385	...	17028.5	CCD	II	+0.0049	-0.0007	(24)
2457865.7105	± 0.0001	17220.0	CCD	I	+0.0074	+0.0014	(25)
2458219.6799	± 0.0001	18356.0	CCD	I	+0.0107	+0.0017	(26)
2458537.9716	...	19377.5	CCD	II	+0.0133	+0.0010	(27)
2458538.1284	...	19378.0	CCD	I	+0.0143	+0.0020	(27)
2458538.2837	...	19378.5	CCD	II	+0.0138	+0.0015	(27)
2458842.2414	...	20354.0	CCD	I	+0.0156	-0.0004	(27)
2458901.1328	± 0.0001	20543.0	CCD	I	+0.0165	-0.0002	(18)

Table 4
(Continued)

JD(Hel.)	Error	Epoch	Method	Type	$(O - C)_i$ (days)	$(O - C)_f$ (days)	References
2458901.2884	± 0.0001	20543.5	CCD	II	+0.0163	-0.0004	(18)
2458903.1579	± 0.0001	20549.5	CCD	II	+0.0163	-0.0005	(18)
2458903.3135	± 0.0001	20550.0	CCD	I	+0.0161	-0.0007	(18)
2459223.1653	...	21576.5	CCD	II	+0.0208	-0.0004	(28)
2459608.2984	± 0.0001	22812.5	CCD	II	+0.0288	+0.0014	(18)
2459636.1856	± 0.0001	22902.0	CCD	I	+0.0287	+0.0008	(18)
2459638.2108	± 0.0004	22908.5	CCD	II	+0.0286	+0.0007	(18)
2459665.1641	± 0.0003	22995.0	CCD	I	+0.0294	+0.0010	(18)

References. (1) Mikolajewski et al. (2003); (2) ASAS epoch; (3) Greaves & Wils (2003); (4) Diethelm (2004); (5) Brát et al. (2008); (6) Hübscher et al. (2010); (7) Diethelm (2009); (8) Hübscher & Monninger (2011); (9) Brát et al. (2009); (10) Nagai (2011); (11) Diethelm (2010); (12) Diethelm (2011); (13) Brát et al. (2011); (14) Nelson (2013); (15) Diethelm (2012); (16) Nagai (2013); (17) Nagai (2014); (18) Present study; (19) Nagai (2016); (20) Hübscher (2017); (21) Samolyk (2016); (22) Nagai (2017); (23) Samolyk (2017); (24) Nagai (2018); (25) Samolyk (2018); (26) Samolyk (2019); (27) Nagai (2020); (28) Nagai (2022).

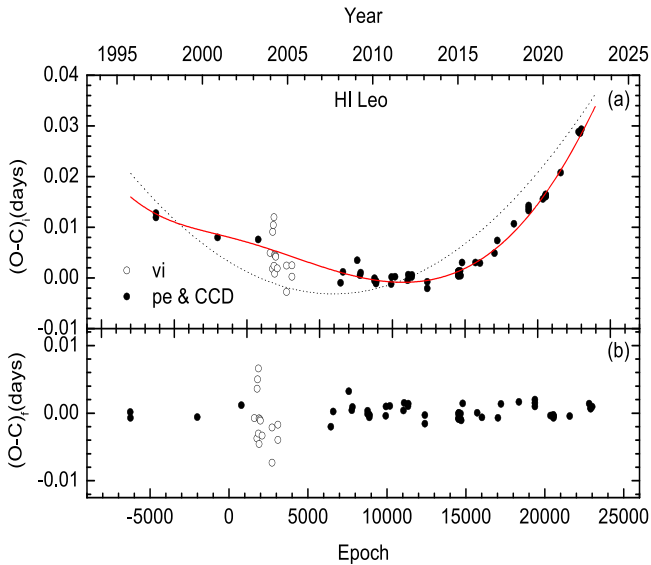


Figure 4. Eclipse residuals, $(O - C)_i$ (a) and $(O - C)_f$ (b) for HI Leo. The continuous and dotted lines represent Equation (2) and its parabolic part, respectively.

4.2. Modeling Light Curves

Six sets of single- or multi-color light curves for two binaries were analyzed by the W-D program (Wilson & Devinney 1971; Wilson 2008). During the solving process, the over-contact configuration (i.e., Mode 3) was always used to obtain the converged solutions. Albedo and gravity darkening coefficients were always $A_{1,2} = 0.5$ and $g_{1,2} = 0.32$ for stars with convective envelopes. According to the effective temperatures of the components and filters used, the limb darkening coefficients were taken from the tables of van Hamme (1993). Several input parameters (i.e., i , T_1 , $\Omega_{1,2}$, L_1), possibly including spot parameters, are adjustable.

4.2.1. HI Leo

Based on the spectral type of $K2V$, we adopted an effective temperature of $T_2 = 4830(\pm 160)$ K and a mass of $M_2 = 0.74(\pm 0.02) M_\odot$ for the more massive component⁸ (Cox 2000), whose error results from a suggested uncertainty of a sub-spectral type. As shown in Figure 2(a), BV light curves of LC_{2020} are almost symmetric, which were used to search for a mass ratio due to the lack of radial velocity curves. We first carried out a series of solutions for some fixed mass ratios ranging from 0.4 to 3.2 with a step of 0.1. The resulting $\Sigma(q)$ is displayed in Figure 7, in which a minimum value of $\Sigma(o - c)_i^2$ occurs around $q = 2.3$. So HI Leo is a W-type contact binary. After the mass ratio is considered a free parameter, we got the final photometric elements, listed in Table 7. The fill-out factor and mass ratio are $f = 6.89(\pm 0.06)\%$ and $q = 2.342(\pm 0.0040)$, which implies that HI Leo is a shallow-contact W-type contact binary.

For another set of light curves LC_{2022} , we neglected the unequal height between two light maxima because B and Rc observations do not cover a whole period, which is displayed in Figure 2(b). After several iterations, we quickly deduced the photometric elements. The temperature of star 1 from LC_{2022} is larger than from LC_{2020} up to $\Delta T_1 = 131$ K, which may result in a sizable variable amplitude and a shallower secondary eclipse in 2022. The Rc light curve from Figure 2(c) displays a large scatter, especially in the light maxima. Similarly, we derived a photometric solution from LC_{2015} , also listed in Table 7. We constructed the corresponding theoretical light curves from three photometric solutions, plotted as continuous lines in Figures 2(a)-(c).

⁸ For the W-type contact binary, star 2 in the W-D code is the cold more massive component, i.e., the primary one.

Table 5
Fitted and Derived Parameters for Period Variations

Parameter	HI Leo	V523 Cas	
	Equation (2)	Equation (2)	the Second LTE
T_0 (HJD)	2452500.1262(6)	2446708.8162(16)	2446708.8151(11)
P (days)	0.31158844(5)	0.23369130(2)	...
Q (days)	$1.22(\pm 0.05) \times 10^{-10}$	$1.11(\pm 0.02) \times 10^{-11}$...
A (days)	0.0066(± 0.0006)	0.0448(± 0.0012)	0.0025(± 0.0002)
e	0.162(± 0.007)	0.071(± 0.002)	0.600(± 0.035)
P_{mod} (yr)	25.74(± 0.95)	114.8(± 2.0)	18.89(± 0.14)
T_s (HJD)	2451101.3(± 177.3)	2429609.9(± 730.3)	2443364.1(± 52.3)
ω (arc)	0.048(± 0.068)	2.428(± 0.062)	4.891(± 0.136)
dP/dt ($\times 10^{-7}$ day yr $^{-1}$)	2.86(± 0.11)	0.345(± 0.007)	...
$\Delta P/P$ ($\times 10^{-6}$)	4.41(± 0.40)	6.71(± 0.18)	2.25(± 0.18)
ΔQ_1 ($\times 10^{49}$ g cm 2)	1.36(± 0.12)	1.51(± 0.04)	0.51(± 0.04)
ΔQ_2 ($\times 10^{49}$ g cm 2)	0.58(± 0.05)	0.78(± 0.02)	0.26(± 0.02)
$a_{12} \sin i$ (au)	1.14(± 0.10)	7.76(± 0.21)	0.433(± 0.035)
$f(m)$ (M_{\odot})	$2.25(\pm 0.06) \times 10^{-3}$	$3.54(\pm 0.03) \times 10^{-2}$	$2.27(\pm 0.05) \times 10^{-4}$
M (M_{\odot})	0.15(± 0.02)	0.45(± 0.01)	0.07(± 0.01)
a_{12} (au)	8.12(± 0.142)	19.7(± 1.0)	7.13(± 1.12)

Table 6
The 120 yr Eclipse Timings of V523 Cas

JD(Hel.)	Error	Method	Epoch	Type	$(O - C)_i$ (days)	$(O - C)_1$ (days)
2415677.852	...	pg	-132787.0	I	+0.2838	-0.0014
2416444.601	...	pg	-129506.0	I	+0.2906	+0.0113
2416514.482	...	pg	-129207.0	I	+0.2978	+0.0190
2417114.689	...	pg	-126638.5	I	+0.2679	-0.0063
2417531.708	...	pg	-124854.0	I	+0.2642	-0.0069
2417622.492	...	pg	-124465.5	I	+0.2590	-0.0114
.....						
2458430.4624	...	CCD	50158.5	I	+0.0639	-0.0004
2459437.2138	...	CCD	54466.5	I	+0.0718	-0.0019
2459461.4005	± 0.0023	pe	54570.0	I	+0.0715	-0.0025
2459461.5187	± 0.0029	pe	54570.5	I	+0.0728	-0.0012
2459461.6340	± 0.0005	pe	54571.0	I	+0.0713	-0.0027
2459465.3674	± 0.0001	CCD	54587.0	I	+0.0656	-0.0084

(This table is available in its entirety in machine-readable form.)

4.2.2. V523 Cas

For the W-type binary V523 Cas, Rucinski et al. (2003) obtained a mass ratio of $q_{\text{sp}} = M_s/M_p = 0.516(\pm 0.007)$ and a spectral type of *K4V*. So we fixed a mass ratio of $q = M_2/M_1 = 1/0.516 \simeq 1.877$ and an effective temperature of $T_2 = 4500$ K (Zola et al. 2010). We first deduced two sections of TESS light curves, LC₁₇₆₈ and LC₁₇₇₉, which are displayed in Figure 3(a). For the symmetric LC₁₇₇₉, we easily derived a photometric solution. For the asymmetric LC₁₇₆₈, the difference between two light maxima is up to $\Delta M_{\text{max}} = -0.014$ mag, which was modeled by a cool spot assuming on the

equator of star 2. The deduced parameters of spot are as follows: colatitude $\phi = 90^\circ$, longitude $\lambda = 108.3(\pm 2.8)^\circ$, angular radius $\gamma = 10.0(\pm 0.9)^\circ$, and temperature factor $T_s/T = 0.89$ (± 0.05). Two photometric solutions from TESS light curves are listed in Table 7. Figure 3(b) plots the corresponding theoretical light curves as continuous lines.

The *V* and *Rc* light curves in 2006 and 2007 only include 83 data in the *V* band and 67 data in the *Rc* band. So we neglected the asymmetry of LC_{*V*Rc} due to low time resolution. LC_{*V*Rc} observations were analyzed simultaneously, and we obtained another preliminary solution, also listed in Table 7. As

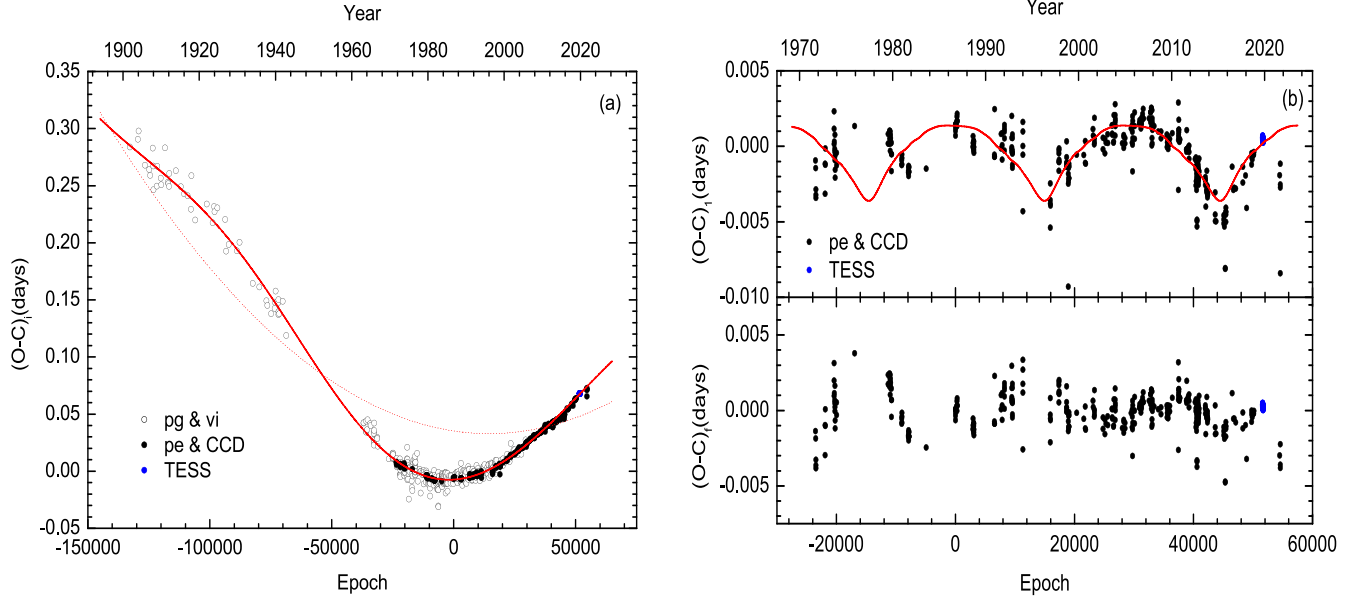


Figure 5. (a) Initial residuals $(O - C)_i$ for V523 Cas. Equation (2) and its parabolic part are plotted by solid and dotted lines, respectively. (b) Residuals $(O - C)_1$ (upper panel) and $(O - C)_f$ (lower panel). The continuous line is the second light-time effect with zero-point.

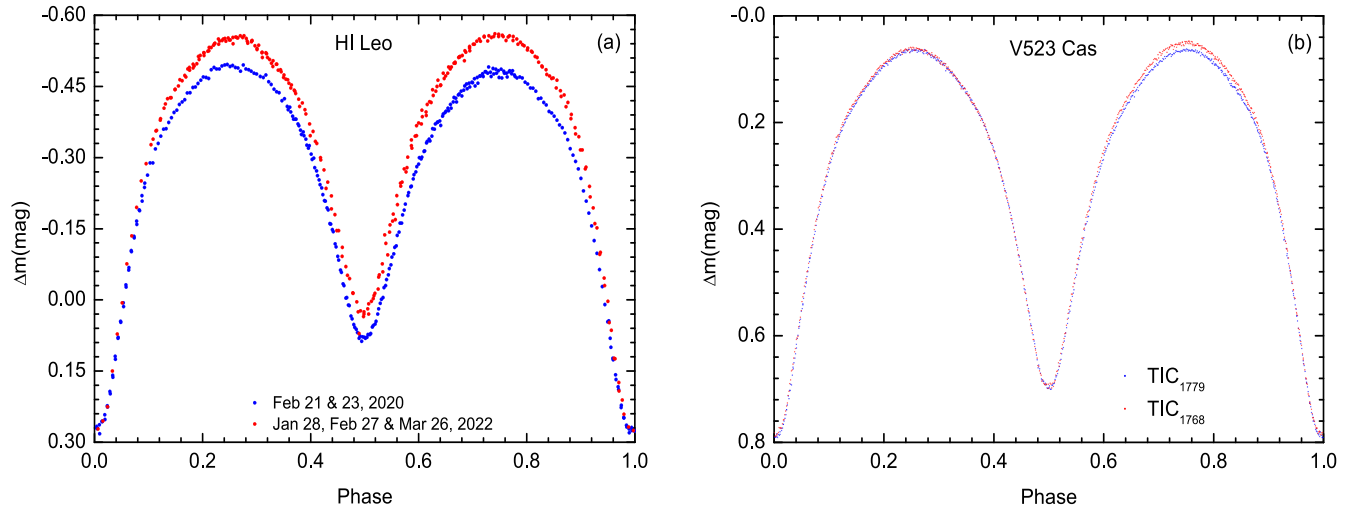


Figure 6. Intrinsic light variabilities with time for HI Leo (a) and V523 Cas (b).

displayed in Figure 2(d), from which the computed light curves fitted observations poorly, especially in the V band.

5. Discussions

5.1. Absolute Parameters and Evolutionary States

We obtained six photometric solutions from the preceding analysis, two of which are accepted as the final ones from LC_{2020} for HI Leo and LC_{1779} for V523 Cas. For HI Leo, we adopted a mass of $M_2 = 0.74(\pm 0.02) M_\odot$ for the more massive component (see Section 3.1). The mass for the less massive

component is $M_1 = 0.32(\pm 0.01) M_\odot$. For V523 Cas, the amplitudes of radial velocities, K_1 and K_2 , are determined by Rucinski et al. (2003). When inserting P , i , K_1 and K_2 into the mass function of $M_{1,2} \sin^3 i / P = 1.0385 \times 10^{-7} (K_1 + K_2)^2 K_{2,1}$, we obtained the masses of M_1 and M_2 . By using Kepler's third law and Stefan-Boltzmann law, we finally (re-)determined other absolute parameters, which are listed at the end of Table 7.

The mass-luminosity relations of the two components are displayed in Figure 8, where the open and solid circles refer to both components of 406 contact binaries (Latković et al. 2021).

Table 7
Photometric Solutions and Absolute Parameters for HI Leo and V523 Cas

Parameters	HI Leo			V523 Cas		
	LC ₂₀₂₀	LC ₂₀₂₂	LC ₂₀₁₅	TIC ₁₇₇₉	TIC ₁₇₆₈	LC _{VRC}
$q = M_2/M_1$	2.342(±0.004)	2.355(±0.004)	2.372(±0.005)		1.877 ^a	
i (°)	80.73(±0.10)	81.70(±0.13)	80.10(±0.15)	81.84(±0.03)	82.04(±0.04)	83.50(±0.12)
$\Omega_{1,2}$	5.6871(±0.0052)	5.6930(±61)	5.6885(±0.0085)	5.0220(±0.0010)	5.0170(±0.0015)	5.0342(±0.0150)
T_1 (K)	5126(±4)	5257(±6)	5245(±8)	4699(±2)	4694(±3)	4664(±19)
T_2 (K)		4830 ^a			4500 ^a	
$^b \ell_1$ (B)	0.4200(±0.0012)	0.4611(±0.0016)	0.4174(±0.0055)
ℓ_1 (V)	0.3979(±0.0010)	0.4296(±0.0012)	0.4053(±0.0045)
ℓ_1 (Rc)	...	0.4071(±0.0010)	0.4046(±0.0013)
ℓ_1 (TESS)	0.4069(±0.0004)	0.4060(±0.0005)	...
r_1 (pole)	0.2909(±0.0010)	0.2909(±0.0010)	0.2933(±0.0011)	0.3098(±0.0015)	0.3101(±0.0015)	0.3086(±0.0018)
r_1 (side)	0.3037(±0.0015)	0.3039(±0.0016)	0.3068(±0.0017)	0.3242(±0.0017)	0.3246(±0.0016)	0.3227(±0.0020)
r_1 (back)	0.3348(±0.0019)	0.3391(±0.0018)	0.3442(±0.0020)	0.3598(±0.0019)	0.3605(±0.0020)	0.3575(±0.0024)
r_2 (pole)	0.4306(±0.0016)	0.4322(±0.0018)	0.4346(±0.0021)	0.4138(±0.0020)	0.4142(±0.0021)	0.4127(±0.0021)
r_2 (side)	0.4596(±0.0020)	0.4616(±0.0023)	0.4647(±0.0024)	0.4399(±0.0023)	0.4404(±0.0023)	0.4385(±0.0028)
r_2 (back)	0.4880(±0.0025)	0.4903(±0.0026)	0.4942(±0.0028)	0.4702(±0.0027)	0.4709(±0.0030)	0.4683(±0.0031)
f (%)	6.89(±0.06)	8.86(±0.09)	13.44(±0.19)	9.22(±0.02)	10.06(±0.03)	7.16(±0.18)
M_1 (M_\odot)	0.32(±0.01)			0.388(±0.004)		
M_2 (M_\odot)	0.74(±0.02) ^a			0.753(±0.005)		
R_1 (R_\odot)	0.90(±0.02)			0.553(±0.003)		
R_2 (R_\odot)	0.61(±0.01)			0.736(±0.004)		
L_1 (L_\odot)	0.40(±0.02)			0.134(±0.001)		
L_2 (L_\odot)	0.23(±0.01)			0.199(±0.002)		

Notes.

^a Adopted the fixed values.

^b Relative luminosities can be expressed by $\ell_{1/2} = L_{1/2}/(L_1 + L_2)$.

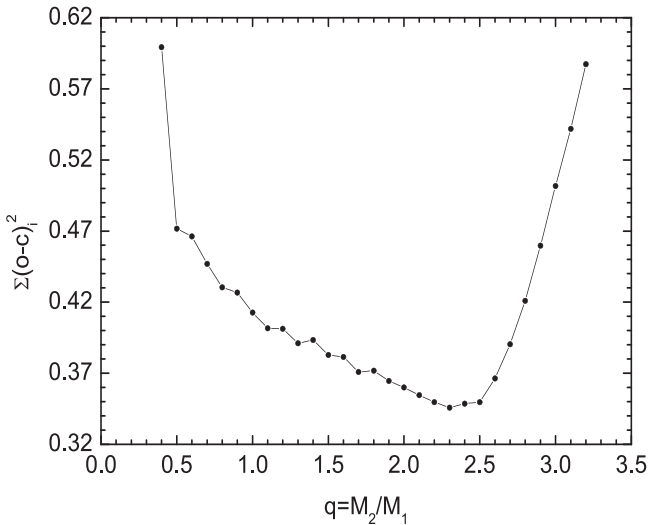


Figure 7. Searching a mass ratio of q from the BV light curves in 2020.

The primaries for two binaries between ZAMS and TAMS lines imply that they are evolved main-sequence stars. Meanwhile, the secondaries lie upon the TZMS line, whose over-luminosities may be attributed to energy transfer for W-type binaries (Zhang et al. 2020b).

5.2. Do Additional Companions Exist in Two K-type Binaries?

Based on the eclipse timing residuals, the orbital periods may suffer from a period increase with one or two light-time effects. This case occurs in other contact binaries, such as Y Sex and V1363 Ori (Yang et al. 2021) and EE Cet (Yang & Wang 2023). The observed periodic oscillations for contact binaries may result from the variation the quadrupole moment of ΔQ (Applegate 1992). We computed ΔQ by the second equation of Lanza & Rodono (2004). As in Table 5, the values are smaller than the typical order of 10^{51} – 10^{52} g cm². Therefore, the mechanism of magnetic activity cycles may not work in two binaries.

We then considered the light-time effect via the presence of the additional body, which causes the observed oscillation. For HI Leo, the semi-amplitude and modulated period are $A = 0.0066(\pm 0.0006)$ and $P_{\text{mod}} = 25.74(\pm 0.95)$ yr, respectively. Using the mass function,

$$f(m) = \frac{(173.145 \times a_{12} \sin i)^3}{P_{\text{mod}}^2} = \frac{(m_3 \sin i)^3}{(M_1 + M_2 + m_3)^2}, \quad (5)$$

we computed the mass and radius of the third body. For V523 Cas, there exist two light-time effects with $A_3 =$

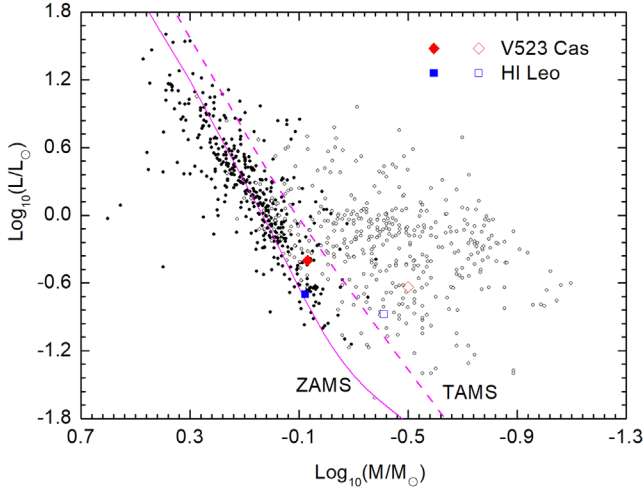


Figure 8. Evolutionary states of the components for two binaries. ZAMS and TAMS lines as continuous and dashed lines were constructed by the *BSE* code (Hurley et al. 2002). Color diamonds and squares represent V523 Cas and HI Leo, respectively.

$0^d0448(\pm 0^d0012)$ and $P_3 = 114.8(\pm 2.0)$ yr for the third body, $A_4 = 0^d0026(\pm 0^d0002)$ and $P_4 = 18.89(\pm 0.14)$ yr for the fourth body, respectively. Because the fourth body lies in the orbit of the third body. We first computed the orbital parameters of the fourth body by Equation (5). Then we derive the parameters of the third body through the revised Equation (5), that is, a_{12} and $M_1 + M_2 + m_3$ are replaced by a_{124} and $M_1 + M_2 + m_4 + m_3$. This kind of method for V523 Cas is similar to RZ Dra (Yang et al. 2010). When the additional companions are coplanar with the binary’s orbit, we derived the mass and radius listed in Table 5. If it is true, HI Leo is a triple system, and V523 Cas is a quintuple system.

5.3. Mass Transfer and Possible Evolutionary Scenarios

We computed the orbital period increase rate from the quadratic coefficient of Equation (2), i.e., $dP/dt = +2.86(\pm 0.11) \times 10^{-7}$ day yr $^{-1}$ for HI Leo and $dP/dt = +2.45(\pm 0.07) \times 10^{-8}$ day yr $^{-1}$ for V523 Cas, respectively. The period increasing may be generally interpreted by mass transfer from the less massive component (i.e., the primary) to the more massive one (i.e., the secondary). Assumed in the conserved mass transfer, its transferring rate can be computed by the following equation,

$$\frac{dM_p}{dt} = \frac{M_s}{3(1-q)} \times \frac{1}{P} \frac{dP}{dt}, \quad (6)$$

where the subscripts of “p” and “s” represent the primary and secondary components. Inserting M_s , $q = M_s/M_p$ and dP/dt into Equation (6), we obtained the mass transfer rate of $dM_p/dt = 1.69(\pm 0.07) \times 10^{-1} M_\odot$ yr $^{-1}$ for HI Leo, and

$dM_p/dt = 3.95(\pm 0.08) \times 10^{-8} M_\odot$ yr $^{-1}$ for V523 Cas, respectively. With mass transferring, the mass ratio decreases, which will cause the inner and outer critical potentials to increase. Finally, the contact degree of contact binary will be decreasing. As predicted by the TRO theory, this kind of W-type binaries with the period increase, HI Leo and V523 Cas, may evolve into broken-contact configurations.

Acknowledgments

Authors would express many thanks for the anonymous referee for his helpful comments and suggestions. Our research was supported by the National Natural Science Foundation of China (Grant No. 11873003). The low-precision spectrum and new photometry for HI Leo were observed by the 2.16 m and the 60 cm telescopes at XLs of NAOC. The *VRc* observations for V523 Cas was performed by the 85 cm telescope at XLs of NAOC and the 1.0 m telescope at YNAO. The continuous photometry for V523 Cas is downloaded from TESS, whose mission is provided by NASA’s Science Mission directorate.

ORCID iDs

Yuanguai Yang  <https://orcid.org/0000-0002-0151-6557>
 Huiyu Yuan  <https://orcid.org/0000-0002-8018-3112>

References

- Agueros, M. A., Anderson, S. F., Covey, K. R., et al. 2009, *ApJS*, **181**, 444
 Andersen, J. 1991, *A&ARv*, **3**, 91
 Applegate, J. H. 1992, *ApJ*, **385**, 621
 Bradstreet, D. H. 1981, *AJ*, **86**, 98
 Brát, L., Šmelcer, L., Kučaková, H., et al. 2008, *OEJV*, **94**, 1
 Brát, L., Trnka, J., Lehky, M., et al. 2009, *OEJV*, **107**, 1
 Brát, L., Trnka, J., Šmelcer, L., et al. 2011, *OEJV*, **137**, 1
 Cox, A. N. (ed.) 2000, *Allen’s Astrophysical Quantities* (4th ed.; New York: Springer), 388
 Diethelm, R. 2004, *IBVS*, **5543**, 1
 Diethelm, R. 2009, *IBVS*, **5894**, 1
 Diethelm, R. 2010, *IBVS*, **5945**, 1
 Diethelm, R. 2011, *IBVS*, **5992**, 1
 Diethelm, R. 2012, *IBVS*, **6029**, 1
 Eastman, J., Siverd, R., & Gaudi, B. S. 2010, *PASP*, **122**, 935
 Eggleton, P. P. 2010, *NewAR*, **54**, 45
 Fan, Z., Wang, H., Jiang, X., et al. 2016, *PASP*, **128**, 5005
 Greaves, J., & Wils, P. 2003, *IBVS*, **5458**, 1
 Henden, A. A., & Stone, R. C. 1998, *AJ*, **115**, 296
 Hübscher, J. 2017, *IBVS*, **6196**, 1
 Hübscher, J., Lehmann, P. B., Monninger, G., et al. 2010, *IBVS*, **5918**, 1
 Hübscher, J., & Monninger, G. 2011, *IBVS*, **5959**, 1
 Hurley, J. R., Tout, C. A., & Pols, O. R. 2002, *MNRAS*, **329**, 897
 Irwin, J. B. 1952, *ApJ*, **116**, 211
 Kouzuma, S. 2019, *PASJ*, **71**, 21
 Kreiner, J. M. 2004, *AcA*, **54**, 207
 Kreiner, J. M., Kim, C.-H., & Nha, H.-S. 2001, *An Atlas of O-C Diagrams of Eclipsing Binary Stars* (Poland: Wydawnictwo Naukowe AP)
 Kwee, K. K., & van Woerden, H. 1956, *BAN*, **12**, 137
 Langer, N. 2012, *ARA&A*, **50**, 107
 Lanza, A. F., & Rodono, M. 2004, *AN*, **325**, 393
 Latković, O., Čeki, A., & Lazarević, S. 2021, *ApJS*, **254**, 10
 Li, H.-L., Wei, J.-Y., Yang, Y.-G., & Dai, H.-F. 2016, *RAA*, **16**, 2
 Liu, L., Qian, S.-B., & Xiong, X. 2018, *MNRAS*, **474**, 5199
 Long, L., Zhang, L.-Y., Han, X., et al. 2019, *MNRAS*, **487**, 5520

- Maithong, W. 2021, *JPhCS*, **1835**, 012099
- Mikolajewski, M., Galan, C., & Graczyk, D. 2003, *IBVS*, **5445**, 1
- Milone, E. F., Hrivnak, B. J., & Fisher, W. A. 1985, *AJ*, **90**, 354
- Mohammadi, M., Abedi, A., & Riazi, N. 2016, *NewA*, **44**, 78
- Nagai, K. 2011, *Var. Star Bull. Japan*, **51**, 1
- Nagai, K. 2013, *Var. Star Bull. Japan*, **55**, 1
- Nagai, K. 2014, *Var. Star Bull. Japan*, **56**, 1
- Nagai, K. 2016, *Var. Star Bull. Japan*, **61**, 1
- Nagai, K. 2017, *Var. Star Bull. Japan*, **63**, 1
- Nagai, K. 2018, *Var. Star Bull. Japan*, **64**, 1
- Nagai, K. 2020, *Var. Star Bull. Japan*, **67**, 1
- Nagai, K. 2022, *Var. Star Bull. Japan*, **91**, 1
- Nelson, R. H. 2013, *IBVS*, **6050**, 1
- O'Connell, D. J. K. 1951, *MNRAS*, **111**, 642
- Özavic, İ., Özuyar, D., Şenavci, H. V., et al. 2020, *AcA*, **70**, 33
- Pickles, A. J. 1998, *PASP*, **110**, 863
- Qian, S.-B., He, J.-J., Zhang, J., et al. 2017, *RAA*, **17**, 87
- Qian, S.-B., Zhu, L.-Y., Liu, L., et al. 2020, *RAA*, **20**, 163
- Ricker, G. R., Winn, J. N., Vanderspek, R., et al. 2015, *JATIS*, **1**, 014003
- Rovithis-Livaniou, H., Tsantilas, S., & Kalimeris, A. 2003, *ASPC*, **292**, 215
- Rucinski, S. M., Capobianco, C. C., Lu, W., et al. 2003, *AJ*, **125**, 3258
- Samec, R. G., Faulkner, D. R., & Williams, D. B. 2004, *AJ*, **128**, 2997
- Samolyk, G. 2016, *JAAVSO*, **44**, 69
- Samolyk, G. 2017, *JAAVSO*, **45**, 121
- Samolyk, G. 2018, *JAAVSO*, **46**, 184
- Samolyk, G. 2019, *JAAVSO*, **47**, 106
- Stępień, K. 2011, *AcA*, **531**, 18
- Stępień, K., & Gazeas, K. 2008, *IAUS*, **252**, 427
- Szczygiel, D. M., Socrates, A., & Paczyński, B. 2008, *AcA*, **58**, 405
- Tylenda, R., Hajduk, M., Kamiński, T., et al. 2011, *A&A*, **528**, 114
- van Hamme, W. 1993, *AJ*, **106**, 2096
- Wang, S., & Yuangui, Y. 2022, *RAA*, **22**, 115004
- Webbink, R. F. 2003, *ASPC*, **293**, 76
- Weber, R. 1957, *BSAF*, **71**, 36
- Wilson, R. E. 2008, *ApJ*, **672**, 575
- Wilson, R. E. 2020, *Galax*, **8**, 57
- Wilson, R. E., & Devinney, E. J. 1971, *ApJ*, **166**, 605
- Yang, Y., & Wang, S. 2023, *NewA*, **98**, 101919
- Yang, Y.-G. 2009, *ScChG*, **39**, 637
- Yang, Y.-G., Li, H.-L., Dai, H.-F., & Zhang, L.-Y. 2010, *AJ*, **140**, 1687
- Yang, Y.-G., Wang, S., Yuan, H.-Y., & Dai, H.-F. 2021, *RAA*, **21**, 290
- Yang, Y., Yuan, H., Wang, S., & Dai, H. 2022, *AJ*, **163**, 250
- Zboril, M., & Djurasevic, G. 2006, *SerAJ*, **173**, 84
- Zhang, L., Lu, H., Han, X. L., et al. 2018, *NewA*, **61**, 36
- Zhang, L., Zhu, Z., Yue, Q., et al. 2020, *MNRAS*, **491**, 6065
- Zhang, X. B., & Zhang, R. X. 2004, *MNRAS*, **347**, 307
- Zhang, X.-D., Qian, S.-B., & Liao, W.-P. 2020, *MNRAS*, **492**, 4112
- Zhou, A.-Y., Jiang, X.-J., Zhang, Y.-P., & Wei, J.-Y. 2009, *RAA*, **9**, 349
- Zhu, L.-Y., Zhao, E.-G., & Zhou, X. 2016, *RAA*, **16**, 68
- Zola, S., Gazeas, K., Kreiner, J. M., et al. 2010, *MNRAS*, **408**, 464